The competition between fracture nucleation, propagation and coalescence in the crystalline continental upper crust

Jessica A. McBeck[1], Wenlu Zhu[2], François Renard[1,3]

[1]Njord Centre, Department of Geosciences, University of Oslo, Norway
[2]Department of Geology, University of Maryland, College Park, U.S.A.
[3]University Grenoble Alpes, University Savoie Mont Blanc, CNRS, IRD, IFSTTAR, ISTerre, France

Correspondence to: Jessica McBeck (j.a.mcbeck@geo.uio.no)

Abstract. Different modes of fracture growth produce fracture networks with distinctive geometric attributes that exert important controls on the extent of fluid-rock interactions. We perform in situ X-ray tomography triaxial compression experiments on monzonite to investigate the influence of fracture nucleation, preexisting fracture propagation, and coalescence on fracture network development in crystalline rocks under crustal conditions. We impose a confining pressure of 20-35 MPa and then increase the differential stress in steps until the rock fails macroscopically. After each stress step we acquire a three-dimensional (3D) X-ray adsorption coefficient field from which we extract the 3D fracture network. To examine the influence of pore fluid on fracture network development, we perform two experiments under nominally-dry conditions and one under water-saturated conditions with 5 MPa pore fluid pressure. We develop a method of tracking individual fractures between subsequent tomographic scans that identifies whether fractures grow from the coalescence and linkage of several fractures or from the propagation of a single fracture. Throughout loading until shortly before failure in all of the experiments, the volume of coalescing fractures is smaller than the volume of propagating fractures, indicating that fracture propagation dominates coalescence. Immediately preceding failure, however, the volume of coalescing fractures is at least double the volume of propagating fractures in the experiments deformed at nominally dry conditions. In the water-saturated sample, although the volume of coalescing fractures increases during this stage, the volume of propagating fractures remains dominant. The influence of stress corrosion cracking associated with hydration reactions at fracture tips and/or dilatant hardening may explain the observed difference in fracture development under dry and water-saturated conditions. Our experimental data on fracture growth at different conditions provide new constraints in assessing fluid flow in subsurface fracture networks that are central to energy and environmental engineering practices.

1. Introduction

Fracture and fault networks develop through the nucleation of new fractures, the propagation of new and preexisting fractures, and the coalescence of neighboring ifractures (e.g., *Olson*, 1993; *Reches & Lockner*, 1994; *Mansfield & Cartwright*, 2001; *Crider & Peacock*, 2004; *Jackson & Rotevatn*, 2013). Formulations of linear elastic fracture mechanics (LEFM) can describe the potential of propagation of one or a few fractures within linear elastic material (e.g., *Griffith*, 1921; *Irwin*, 1957).

However, these analytical formulations focus on fractures significantly larger than the length of preexisting defects that permeate rocks. Thus, they provide few insights into the coalescence behavior of fracture networks as they transition from distributed, disperse networks comprised of many isolated, small fractures to more localized networks comprised of well-connected, larger fractures. These formulations also struggle to compare the competing influence of three endmember fracture 35 growth modes on fracture network development: 1) nucleation, 2) isolated propagation and 3) coalescence.

Identifying which of these modes dominates the others under varying conditions can be critical for accurate assessment of fracture network development. For example, if nucleation is the dominant mode of fracture development rather than isolated propagation, then using metrics that identify sites of potential fracture nucleation may be more successful than using metrics that predict the conditions under which a preexisting fracture will grow. The corresponding predicted propagation directions 40 may differ depending on the mode of failure.

Metrics that indicate regions in which fractures may nucleate include the strain energy density, maximum Coulomb stress, maximum magnitude of shear stress, and highest tensile stress or least compressive stress (e.g., *Jaeger et al.*, 1979; *Atkinson*, 1987; *Du & Aydin*, 1993). Previous analyses have used some of these metrics to predict the direction of fracture growth from a preexisting fracture tip (e.g., *Olson & Cooke*, 2005; *Okubo & Schulz*, 2005; *Fattaruso et al.*, 2016). However, these metrics 45 can lead to conflicting predictions about both the sites of new fracture nucleation and the direction of fracture growth (e.g., *Madden et al.*, 2017; *McBeck et al.*, 2017, 2020). If preexisting fracture propagation is the dominant mode of development rather than fracture nucleation, then metrics that determine the conditions under which preexisting fractures will grow, such as the critical stress intensity factor (*Isida*, 1971), and the direction of this fault growth, such as Coulomb shear stress, tensile stress, and energy optimization (e.g., *Pollard & Aydin*, 1988; *Müller,* 1988; *Mary et al.*, 2013; *Madden et al.*, 2017; *McBeck* 50 *et al.*, 2017), may provide more accurate predictions of fault network development than nucleation criteria. Determining which mode dominates deformation under varying conditions may help identify analyses suitable for successful prediction of fracture network development.

Some of the aforementioned criteria used to identify the sites of fracture nucleation, and the conditions, rate, and geometry of growth from preexisting fractures may also be extended to study coalescence. Indeed, at least one fracture must propagate 55 or open to allow coalescence. Thus, the factors that promote coalescence are also those that promote propagation, such as higher strain energy density, and so these criteria may not provide a clear method of distinguishing between the dominance of isolated propagation or coalescence. The question of whether a fracture network is dominated by many isolated fractures or several connected fractures that form via coalescence can profoundly affect the rate and extent of fluid-rock interactions. For two rocks with the same porosity, the rock with a more distributed fracture network may provide more surface area available 60 for chemical reactions than the rock with more localized networks consisting of a few larger fractures. Consequently, fluid-rock interactions in the rock with many distributed small fractures will likely be more effective than in one with a few large fractures. Thus, identifying the conditions under which coalescence or isolated propagation dominates may help assess the efficiency of geothermal energy and unconventional fossil fuel productions, and identify sites ideal for waste disposal or CO_2 sequestration.

65   To investigate the relative contributions of these deformation modes to fracture network development, we quantified the evolution of 3D fracture networks in monzonite samples undergoing brittle failure using in situ dynamic X-ray synchrotron microtomography. We conducted three triaxial deformation experiments at room temperature and confining pressures of 20-35 MPa. In two of the experiments the sample was deformed at nominally dry conditions. In the third experiment the sample was saturated with deionized water and deformed at a constant pore fluid pressure of 5 MPa under drained conditions. During

70   the deformation tests, the maximum principal (compressive) stress σ_1 was increased in distinct steps of 1-5 MPa while the intermediate and minimum principal stresses $\sigma_2 = \sigma_3 = 20 - 35$ MPa were kept constant until macroscopic failure occurred (**Figure** 1). After each differential stress (σ_1 - σ_2) increase, we acquired a microtomographic scan of the deforming rock at in situ stress conditions. From the microtomographic datasets, we obtained the evolving three-dimensional (3D) fracture networks within the samples (**Figure** 2). We developed new methods of tracking the growth of fractures that enable distinguishing

75   between fractures that grow via isolated propagation and those that grow from the coalescence of several fractures. Our results demonstrate that the competing influence of 1) nucleation and preexisting propagation, 2) isolated propagation and coalescence, and 3) local stress perturbations evolve toward macroscopic failure and depend on the stress states and interstitial fluid.

2.   Methods

80   **2.1. In situ X-ray tomography**

        We performed three triaxial deformation experiments with in situ dynamic X-ray synchrotron microtomography at beamline ID19 at the European Synchrotron and Radiation Facility (ESRF). We deformed monzonite cylinders 1 cm in height and 0.4 cm in diameter. In each experiment, we imposed a constant confining pressure ($\sigma_2 = \sigma_3$) and then increased the axial stress (σ_1) in steps until the rock failed macroscopically. After each differential stress increment, we acquired a scan of the

85   sample at in situ stress conditions (*Renard et al*., 2016). The duration of each scan is within 2 minutes (**Figure** 1, **Figure** 2). The experiments were conducted at room temperature, at three different confining pressures: 20 MPa (experiment #3), 25 MPa (#5), and 35 MPa (#4). Macroscopic failure occurred in a sudden stress drop. The final scan was taken at a differential stress very close to the failure stress, typically <0.5 MPa below the failure stress. Experiments #3 and #5 were conducted at nominally dry conditions, while in experiment #4 the sample was fully saturated. This sample was submerged in deionized water for 24

90   hours under vacuum before the experiment to help ensure that the pore space was saturated. In experiment #4, a constant pore fluid pressure of 5 MPa was maintained using two pore pressure pumps connected at each end of the sample (top and bottom). Experiment #4 is also unique in that we reached the axial stress limit of the device (200 MPa) preceding macroscopic failure, and thus we reduced the confining pressure in steps of 1 MPa from 35 to 31 MPa until the core failed. Consequently, the sample experienced 35 MPa of confining pressure for 60 scans and stress steps, and then experienced 34 MPa, 33 MPa, 32

95   MPa, and 31 MPa confining pressure in the final four scans preceding failure, respectively. The X-ray tomography data of the

three experiments are publicly available (*Renard*, 2017, 2018). *Renard et al*. (2018, 2019b) describe the experimental conditions in further detail.

2.2. Extraction of fracture network

From the time series of 3D adsorption coefficient fields acquired throughout loading, we identify fractures and pores using
100   a standard thresholding technique. The histogram of grey-scale values from a tomogram of a porous rock tends to have two maxima indicative of the modes of the solid and air (or deionized water) populations, respectively (e.g., *Renard et al*., 2019a). The local minimum of this histogram then determines the threshold that indicates whether voxels are identified as pore space or solid. Segmenting the tomograms with this procedure yield 3D binary fields of zeros and ones that indicate whether a voxel is within or outside of a fracture or pore. Because we employ the same threshold throughout loading in each experiment, the
105   choice of the threshold has a similar effect for the entire time series of scans.

From the binary field, we extract individual fracture or pore objects by identifying groups of voxels that have 26-fold connectivity, the highest degree of connectivity in 3D. For each group of voxels, we calculate the covariance matrix and corresponding eigenvectors and eigenvalues, which approximate these volumes as ellipsoids. We then use each ellipsoid as approximated fracture and pore objects in subsequent analyses. For all of the calculations using the fracture volume, we use
110   the (more accurate) volume of the group of connected voxels, rather than the ellipsoid volume. For all calculations that depend on the placement of the fractures in space, we use the ellipsoids.

2.3. Identifying propagating and coalescing fractures

After identifying the individual fractures at each loading step of an experiment, we now track the fractures in different tomographic datasets across several loading steps. In addition, we develop a method that links one or more fractures at the
115   previous loading step (t_n) to the next loading step (t_{n+1}) (**Figure** 3). This development is the central difference between this new method and the previous method of tracking fractures in X-ray tomography data developed by *Kandula et al*. (2019). The previous method did not allow linking more than one fracture in t_n to a fracture in t_{n+1}. Thus, *Kandula et al*. (2019) could identify when an individual fracture gained or lost volume from one loading step (and tomogram) to the next. However, this analysis could not differentiate between fractures that gained volume because one fracture propagated and opened, or because
120   several fractures propagated and linked with each other (i.e., coalesced).

We developed a method of tracking fractures in order to examine the competing influence of fracture coalescence and isolated propagation (**Figure** 3). Our new method identifies one or more fractures in t_n and one fracture in t_{n+1} by searching for fractures in t_n that are within five voxels of a fracture in t_{n+1}. We use the ellipsoidal approximations of the fractures to do this search. The limit of five voxels helps ensure that the algorithm identifies fractures that have shifted in space due to
125   deformation. The appropriate value of this limit may differ in rocks that experience differing axial and radial strains in each loading step those observed here. We only perform the analysis for fractures with volumes >100 voxels. This volume threshold helps exclude noise from the analysis. The appropriate volume threshold is likely different for rocks that host differing ranges

of fracture volumes than those observed here. Varying the volume threshold (from 100 to 500 voxels) does not change the main trends described in the results (**Figure** S1).

3. Results

3.1. Macroscopic mechanical behavior

The global mechanical behavior captured in the differential stress and axial strain relationships indicates that the monzonite samples undergo the deformation stages typical for brittle materials under triaxial compression (e.g., *Paterson & Wong*, 2005). We may separate the deformation behaviors into four different stages. Stage I is the initial non-linear stage corresponding to closure of pre-existing defects. Stage II includes a quasi-linear relationship between stress and strain, when the deformation can be approximated as elastic. Stage III occurs when deformation behavior deviates significantly from linear elasticity. The yield point marks the boundary between stages II and III. Stage IV occurs shortly before macroscopic failure, when the effective elastic modulus is near zero (**Figure** 1). In subsequent sections we discuss how the fracture networks develop during each stage. **Figure** 1 shows the axial strains when the initial shallowing occurs, which we refer to as the yield point in the subsequent text. We mark the yield point using the largest axial strain at which the difference between the observed differential stress and differential stress predicted from a linear fit is less than 1% of the observed differential stress (**Figure** S2). We note that we leave the timing of the transitions from stage I to II and from stage III and IV as only qualitative in the subsequent analysis, while the transition from stage II to III is more precisely defined.

3.2. Fracture nucleation and pre-existing fracture propagation

Here we assess the dominance of fracture nucleation relative to the growth of preexisting fractures throughout loading in the three experiments (**Figure** 4). We track the number and total volume of fractures identified in a loading step that did (i.e., preexisting) and did not (i.e., nucleating) grow from a preexisting fracture identified in the previous loading step. In this and subsequent analyses, data reported for the time closest to macroscopic failure reflect the fracture network development that occurs from the second to last (t_{f-2}) and final (t_{f-1}) scan acquired in the experiment, where t_f is the time of macroscopic failure. The final scan is acquired very close to failure, at a differential stress <0.5 MPa below the peak stress.

Throughout stages I-II in each experiment, both the number and total volume of preexisting and nucleating fractures increase with increasing strain at comparable levels (**Figure** 4). We consider the rate of growth as the increase in number or volume of fractures per strain increment. An increase/decrease in rate of growth thus marks an acceleration/deceleration in fracture growth in terms of number or volume. During the transition from stage II to III at yielding, the number and volume of the preexisting fractures accelerate, whereas the number and volume of nucleating fractures do not accelerate as quickly. Due to this bifurcation in acceleration, the preexisting fractures exceed the nucleating fractures both in number and in volume at the end of stage III and through stage IV, prior to failure (**Figures** 4a, b). At the end of stage IV, the volume of preexisting fractures exceeds the volume of newly nucleating fractures by several orders of magnitude (**Figure** 4b, c). In particular, at the

end of stage VI the volume of newly nucleating fractures is 1%, <1%, and 13% of the volume of preexisting fractures in

160 experiments #3, #5 and #4, respectively. Overall, preexisting fracture propagation dominates fracture nucleation in monzonite rocks deformed to failure.

Our results show that while the acceleration in the number of preexisting fractures coincide with the yield point, the acceleration in the volume of preexisting fractures becomes significant only during stage IV, when macroscopic failure is imminent. This trend may also occur for the nucleating fractures, but the number of nucleating fractures identified near the

165 yield point is too low to draw the conclusion with confidence. Finally, the function of preexisting fracture volume relative to axial strain is approximately constant in linear-log strain-volume space (**Figure** 4c), indicating an exponential increase in total volume as a function of axial strain.

3.3. Isolated fracture propagation and fracture coalescence

To assess the influence of isolated fracture propagation relative to coalescence on fracture network development, we

170 develop a method to recognize when fractures develop from the merger of two or more fractures (i.e., coalescence) or from the lengthening, opening or closing of only one fracture (i.e., isolated propagation). **Figure** 5 shows the number and total volume of fractures identified as coalescing from two or more fractures (i.e., coalescing) or developing from only one preexisting fracture (i.e., propagating). We use the short-hand term *propagating* to indicate fractures that grow in isolation, but we note that fractures identified as coalescing also propagate before or while they merge.

175 The number of propagating fractures is larger than the number of coalescing fractures throughout loading in each experiment (**Figure** 5a). The number and volume of the propagating fractures accelerate throughout stages II-IV. In contrast, the number and volume of the coalescing fractures only appear to accelerate following yielding, throughout stages III-IV. Overall, the differences in number and volume of propagating and coalescing fractures grow larger during stages I-III.

At the end of stage IV immediately preceding macroscopic failure, the total volume of coalescing fractures exceeds the

180 total volume of propagating fractures in the nominally dry experiments (experiments #3 and #5). During this stage, the volume of propagating fractures is 44% or 23% of the volume of coalescing fractures for experiments #3 and #5, respectively. In contrast, in the water-saturated experiment (#4), the total volume of coalescing fractures never exceeds the total volume of propagating fractures. Immediately preceding macroscopic failure, the volume of propagating fractures is about seven times higher than the volume of coalescing fractures in this experiment.

185 **3.4. Disperse and localized fracture growth**

To characterize the influence of localization and stress perturbations on fracture network development, we identify the fractures that are gaining and losing volume from one loading step to the next, i.e., growing or closing, and whether they are located near or far from another fracture. Analytical formulations of LEFM suggest that fractures perturb their local stress field to a distance on the order of their length (e.g., *Chinnery & Petrak*, 1968; *Segall & Pollard*, 1980; *Atkinson*, 1987; *Davy et al.*,

190 2010, 2013). A corollary of this concept is that fractures that are within one fracture length of other (perturbing) fractures may

be more likely to grow, and less likely to close. This behavior will only be true if the local stress perturbation is favorable for growth. In contrast, local stress perturbations can also produce stress fields that hinder fracture growth, i.e., stress shadows. In this case, if a fracture lies in a stress shadow, it should be less likely to grow, and perhaps more likely to close. We test these inferences here. In particular, we track the number of growing and closing fractures that do (i.e., near) and do not (i.e., far) have other fractures within one fracture length of them at each stress step (**Figure** 6). For example, if one fracture (fracture #1) is located within y distance of another fracture (#2) with length y, then fracture #1 is counted in the near category.

The number of growing fractures matches the number of closing fractures in stages I-II early in loading (**Figure** 6a). During stage III after yielding, the number of growing fractures accelerates while the number of closing fractures remains at similar values. The number of growing fractures that are located near other fractures (within a fracture length of them) increases with loading (**Figure** 6b). In contrast, the number of growing fractures that are far from other fractures remains roughly constant throughout loading. These varying trends produce two patterns of fracture growth before and after the yield point. In stages I-II before yielding, the number of growing fractures located far from other fractures exceeds or is similar to the number of growing fractures located near other fractures. These observations do not match the expectations from LEFM, which suggest that fractures located closer to other fractures will be more likely to grow. In stages III-IV after yielding, the number of growing fractures located near to other fractures increasingly exceeds the number of growing fractures located far from other fractures. At the end of stage IV immediately preceding macroscopic failure in all three experiments, the number of growing fractures located near to others is 3-5 times higher than the number growing far from others. When macroscopic failure becomes imminent, the observations match the expectations of LEFM.

The evolution of the number of growing fractures located near to others further highlights the influence of coalescence on fracture network development (**Figure** 6b). The number of these fractures decreases in the final loading steps just before failure in the dry experiments (#3 and #5). In contrast, the number of these fractures continually increases in the water-saturated experiment (#4). Fracture coalescence reduces the total number of fractures as many smaller fractures merge into a few larger fractures.

4. Discussion

4.1. The micromechanisms responsible for brittle failure

Analysis of microstructures of deformed samples and acoustic emissions produced in triaxial compression experiments support the idea that fracture development is primarily responsible for the strain softening observed in during brittle failure (e.g., *Lockner et al*., 1991; *Menéndez et al*., 1996; *Baud et al*., 2004; *Stanchits et al*., 2006; *Benson et al*., 2007; *Aben et al*., 2019). These experiments document maxima in the acoustic emission rate or accelerations in the cumulative acoustic emission count coincident in time with the first stress drop or macroscopic failure. Similarly, early in situ X-ray tomography experiments find that the peak differential stress and subsequent stress drop occurred shortly after the formation of the first visible fractures on the surface of dry Westerly granite (*Kawakata et al*., 1997).

Unlike acoustic emission data, our data enables directly comparing the timing of yielding with the acceleration of fracture network development, and the competing modes of development. Our results show that the yield point coincides in time with

225   the acceleration of the number of fractures, but the exponential growth of the fracture volume initiates before yielding (**Figures** 4-6). Thus, the yield point observed from macroscopic measurements of stress and strain may simply indicate when fracture development reaches some critical volume threshold that produces a non-negligible effect on the effective elastic modulus.

4.2. The competition between fracture nucleation and pre-existing fracture propagation

In these monzonite rocks undergoing brittle failure, preexisting fracture propagation dominates fracture nucleation after

230   yielding (**Figure** 4). At a macroscopic scale, many of the conditions that favor fracture nucleation also favor preexisting propagation, such as higher differential stress and/or lower effective confinements. At a more local scale, mechanical heterogeneities control the location of fracture nucleation and the growth of preexisting fractures. For example, in granular cohesive rocks, such as sandstone, shear and/or tensile stress concentrations at the boundary of grains can promote fracture nucleation (e.g., *Menéndez et al.*, 1996; *Baud et al.*, 2004; *Zhu et al.*, 2010). Similarly, contacts between layers of varying

235   elastic moduli, such as layered sedimentary units, can provide ideal sites of fracture nucleation (e.g., *Underwood et al.*, 2003). These mechanical controls also influence the ability of fractures to propagate following nucleation: fractures can arrest at grain boundaries and mechanical contacts, depending on the degree of stress transfer across such interfaces (e.g., *Cooke & Underwood*, 2001; *McBeck et al.*, 2019a, b). Thus, the competing influence of these modes of fracture network development (nucleation or preexisting propagation) is difficult to predict in rocks that include such mechanical heterogeneities. Granular

240   rocks may contain mechanical heterogeneities that concentrate shear and/or tensile stresses more effectively than monzonite, which consists of an interlocking crystalline structure with relatively homogeneous mechanical properties. For example, numerical discrete element method models of sandstone indicate that the degree of strength heterogeneity between grain boundaries and intragranular material controls the proportion of fractures that nucleate at grain boundaries and those that nucleate within grains (*McBeck et al.*, 2019b). Thus, in a given sandstone volume there will likely be a greater number of sites

245   of significant stress concentrations than in a monzonite or granite volume, and thereby a larger number of sites primed for fracture nucleation. Consequently, we may expect a greater dominance of nucleation in sandstone and other rocks with strong strength heterogeneity than observed in these monzonite rocks.

In the crust, interfaces between mechanical sequences can have a first order effect on the extent of fracture propagation. In sedimentary volumes consisting of parallel layers, for example, mechanical interfaces can arrest fracture growth (e.g., *Cooke*

250   *& Underwood*, 2001; *Underwood et al.*, 2003). When these interfaces inhibit growth in sedimentary sequences undergoing layer-parallel extension, the competition between fracture nucleation and propagation follows a systematic evolution. In these systems, new fractures continually nucleate, propagate perpendicular to the maximum tensile direction, open parallel to this direction, and arrest their propagation at an interface so that eventually the spacing between fractures is proportional to the layer thickness (e.g., *Nar & Suppe*, 1991). When the spacing between fractures reaches a certain critical value, the layer

255   becomes saturated such that no (or few) fractures nucleate and only the preexisting fractures open in order to accommodate

the applied extension (e.g., *Wu & Pollard*, 1995). Thus, early in loading fracture nucleation dominates, and later in loading preexisting fracture development dominates.

260   Here, we document how the competition between fracture nucleation and preexisting development evolves with increasing differential stress in triaxial compression, similar to the evolution observed in extending layered sedimentary sequences. Our results indicate that increasing differential stress promotes the dominance of preexisting fracture development rather than nucleation. As the fractures lengthen and open under increasing differential stress, the stress intensity factors at their tips increase (*Isida*, 1971) and thereby further promote propagation. As deformation localizes among several larger fractures, the energetic cost of propagating preexisting fractures may become less than the cost of nucleating new fractures (e.g., *Del Castello & Cooke*, 2007; *Herbert et al.*, 2015). Our data support these predictions from the linear elastic fracture mechanics and energy

265   optimization.

4.3. The competition between isolated fracture propagation and coalescence

Tracking the volume of fractures that coalesce from several fractures and those that propagate in isolation without merging indicates that isolated propagation dominates coalescence throughout most of the deformation process preceding macroscopic failure (**Figure** 5). Preceding macroscopic failure, our results suggest that the presence of fluid and magnitude of confining

270   stress may affect the competition between isolated propagation and coalescence. We deformed the water-saturated sample (experiment #4) with the highest effective confining stress; the confining pressure minus pore fluid pressure was 30 MPa. In this experiment, the total volume of coalescing fractures was <10% of the volume of propagating fractures immediately preceding macroscopic failure (**Figure** 5b). In contrast, preceding failure in the experiments deformed at lower confining stress (20 and 25 MPa in experiments #3 and #5, respectively), the total volume of coalescing fractures is at least twice the volume

275   of the propagating fractures. This difference in behavior suggests that dry conditions and lower confining stress promote coalescence rather than isolated propagation.

Many observations indicate that the magnitude of confining stress influences fracture development. In porous sandstones, sufficiently high confinement inhibits brittle failure and produces cataclastic flow (e.g., *Wong et al.*, 1997). In the endmember case when a rock undergoes uniaxial compression (i.e., zero confinement), experiments show that opening mode and tensile

280   failure dominate deformation with little evidence of shear deformation (e.g., *Lin et al.*, 2015). With increasing confinement, fractures can appear to rotate from the orientation preferred under uniaxial compression conditions (parallel to the maximum compression direction), toward the range of orientations predicted by the maximum Coulomb shear stress (e.g., *Mair et al.*, 2002). This apparent rotation from parallel to more inclined to the maximum compression direction also occurs in triaxial compression experiments with increasing differential stress (e.g., *McBeck et al.*, 2019a). Analyses often interpret such rotation

285   to indicate an increasing dominance of shear deformation at the expense of tensile deformation. However, such apparent rotation may occur as many individual mode-I fractures link together so that the macroscopic trend of the fault is inclined relative to the maximum compression direction (e.g., *Peng & Johnson*, 1972; *Lockner et al.*, 1991). Consequently, the fracture geometry alone may not indicate the relative proportion of shear and tensile deformation.

Analysis of the moment tensors of acoustic emissions provides further insights to the relative proportion of shear and

290   tensile deformation under varying confining stresses. Analysis of acoustic emissions during triaxial compression suggests that decreasing confining stress promotes tensile failure and opening at the expense of shear failure (e.g., *Stanchits et al.*, 2006). This opening may enable greater access to preexisting fractures than shear deformation, thereby promoting the likelihood of coalescence. For example, mixed-mode fractures may tend to have larger apertures than fractures dominated by shear deformation. Consequently, mixed-mode failure may result in thicker fractures that provide greater surface area to which other

295   fractures can link than thinner fractures produced predominately by shear. The presence of damage zones surrounding crustal faults and the decreasing of the thickness of these damage zones with depth support the idea that confining stress localizes deformation in low porosity crystalline rock. In particular, the flower-shaped structures of crustal faults observed in geophysical data indicate that damage zones can become narrower with increasing depth (e.g., *Harding*, 1985). Confining stress tends to reduce the proportion of tensile deformation relative to shear deformation, and thus may localize deformation

300   into thinner zones, in the absence of cataclastic flow and ductile deformation.

The applied confining pressure in experiment #5 was 5 MPa higher than that of experiment #3, but the two dry samples show similar proportions of fracture propagation and coalescence. Consequently, it is unlikely that the 5 MPa higher effective stress of experiment #4 compared to experiment #5 is the primary trigger of the different behaviors observed in these experiments. We suggest that the presence of water is responsible for the transition from isolated propagation to coalescence-

305   dominated fracture network development. Chemical reactions at fracture tips can influence fracture propagation. Such stress corrosion cracking occurs when chemical reactions reduce the fracture toughness and thereby promote crack propagation (e.g., *Anderson & Grew*, 1977). When water is present, hydrogen bond formation weakens the Si-O bond in quartz-rich sandstones, producing water-weakening (e.g., *Baud et al.*, 2000). In addition, solution transfer at highly stressed contacts can enhance the compaction of limestone when water is present (*Lisabeth & Zhu*, 2015). Stress corrosion cracking may promote nucleation at

310   the expense of coalescence in the water-saturated monzonite experiment.

Changes in pore fluid pressure can also affect the fracture propagation rate (*Ougier-Simonin & Zhu*, 2013, 2015). Recent studies show that at the same effective pressure and loading, fault propagation in intact serpentinite is slower in samples with higher pore fluid pressures (*French & Zhu*, 2017). When a fluid-saturated rock dilates, the pore pressure may drop and thereby reduce the local effective confinement and strengthen the rock, i.e., dilatant hardening (e.g., *Brace & Bombolakis*,1963; *Rice*,

315   1975; *Rudnicki & Chen*, 1988; *Ikari et al.*, 2009; *Xing et al.*, 2019; *Brantut*, 2020). This strengthening can then slow the rate of fracture propagation from dynamic to quasi-stable (*French & Zhu*, 2017). Dilatant hardening can operate in intact rock as well as saturated gouge zones (*Ikari et al.*, 2009; *Xing et al.*, 2019). For example, increasing pore pressure causes the frictional behavior of antigorite gouge to evolve from velocity-weakening to -strengthening (*Xing et al.*, 2019). Dilatant hardening may influence fracture development in the water-saturated experiment #4. However, further experimental investigations are needed

320   to distinguish between the relative importance of stress corrosion cracking and dilatant hardening on the fracture development behaviors of water-saturated rocks.

These observations and our analyses suggest that the presence of water (producing stress corrosion) and high pore fluid pressure (producing dilatant hardening) promote slower, more isolated fracture network growth, rather than faster, coalescence-dominated growth. Understanding the mechanical and chemical conditions that favor one mode of fracture growth over another (e.g., fracture coalescence versus isolated fracture propagation) has important implications in many energy and environmental engineering practices. For example, when their connected porosities are comparable, fracture networks produced by the propagation and coalescence of many small fractures may have higher tortuosity and lower permeability than networks consisting of a few large fractures. However, the fracture networks consisting of numerous small fractures may be more efficient in shale gas exploration and CO_2 sequestration (e.g., *Xing et al.*, 2018).

4.4. The influence of local stress perturbations on fracture growth

A clear factor in fracture network development is the fracture network density, clustering, or localization. For example, earthquakes are more likely to arrest at the ends of faults that are >5 km from another fault (*Wesnousky*, 2006). Indeed, the distance between fractures is one of the key parameters that predicts whether they grow or close from one stress step to the next in X-ray tomography triaxial compression experiments on marble, monzonite and granite rocks (*McBeck et al.*, 2019a). Analytical solutions from LEFM provide a mechanical interpretation of these observations. These solutions indicate that a fracture will perturb the local stress field to a distance on the order of their length (e.g., *Atkinson*, 1987). Following this idea, we would expect that fractures located within this threshold to another fracture will be more likely to grow than fractures outside this threshold.

Our observations match the expectations of LEFM during stages III-IV preceding macroscopic failure (**Figure** 6). During these stages, the number of fractures that grow and are located within the threshold of a fracture length exceeds the number of fractures that grow and are located outside this threshold. Preceding yielding, however, similar numbers of growing fractures are located both within and outside this threshold. When the fracture network is more diffuse under lower differential stress, the distance between fractures does not appear to influence whether a fracture grows or closes. When the fracture network becomes more clustered, the distance between fractures influences whether a fracture grows or closes. Our results highlight the conditions under which LEFM solutions apply in rocks under triaxial compression that host fracture networks with a variety of spatial distributions.

5. Conclusions

In situ dynamic X-ray tomography during the triaxial compression of crystalline rocks reveals the competing influence of three modes of fracture network development: 1) nucleation, 2) isolated propagation and 3) coalescence. We find that the influence of these modes evolves throughout loading, with clear transitions near yielding and macroscopic failure. Preexisting fracture propagation, including isolated propagation and coalescence, becomes the dominant mode of deformation following yielding. Coalescence then becomes the dominant mechanism of fracture network development in dry samples under lower confinements only in the stage close to macroscopic failure. Isolated propagation remains the dominant mechanism throughout

loading in a water-saturated sample under higher confinement. Compared to the LEFM prediction that fractures perturb their
355 local stress field to a distance on the order of their length (e.g., *Atkinson*, 1987), our observations only match these expectations
in the stages of the experiments between yielding and macroscopic failure. Preceding yielding, however, the fractures that are
growing are not significantly closer to other fractures, as predicted by LEFM. When the rock experiences lower differential
stress and the fracture network is more distributed, 1) similar numbers of new fractures nucleate and preexisting fractures
grow, 2) isolated propagation dominates coalescence, and 3) local stress perturbations do not appear to promote fracture growth
360 (**Figure** 7). When the rock experiences higher differential stress following yielding, 1) preexisting fracture propagation
dominates new fracture nucleation, 2) coalescing fracture volume exceeds propagating fracture volume in dry samples when
macroscopic failure is imminent, and 3) local stress perturbations promote fracture growth.

Data availability. The data are available on the Norstore repository (*Renard*, 2017, 2018).

365 *Author contributions*. JM and FR performed the experiments, analyzed results, and wrote the manuscript. WZ analyzed results
and wrote the manuscript.

Competing interests. There are no competing interests.

Acknowledgements. We thank Elodie Boller, Paul Tafforeau, and Alexander Rack for providing advice on the design of the
tomography setup, Benoît Cordonnier for experimental expertise, and Sanchez Technology for building the deformation
370 apparatus. The Research Council of Norway (awards 272217 to FR and 300435 to JM) and U.S. National Science Foundation
(EAR-1761912 to WZ) funded this work. The European Synchrotron Radiation Facility allocated beamtime (Long Term
Proposal ES-295).

References

Aben, F. M., Brantut, N., Mitchell, T. M., and David, E. C.: Rupture Energetics in Crustal Rock From Laboratory-Scale
375 Seismic Tomography. Geophysical Research Letters, 46(13), 7337-7344, 2019.

Anderson, O. L. and Grew, P. C.: Stress corrosion theory of crack propagation with applications to geophysics, Rev. Geophys.
Space Phys.15, 77– 104, 1977.

Atkinson, B. K.: Fracture Mechanics of Rock, 534, Academic, London, 1987.

Baud, P., Klein, E., and Wong, T. F.: Compaction localization in porous sandstones: spatial evolution of damage and acoustic
380 emission activity. Journal of Structural Geology, 26(4), 603-624, 2004.

Baud, P., Zhu, W., Wong, T.-F.: Failure mode and weakening effect of water on sandstone. Journal of Geophysical Research,
105, 16,371-16,389, 2000.

Benson, P. M., Thompson, B. D., Meredith, P. G., Vinciguerra, S., and Young, R. P.: Imaging slow failure in triaxially deformed Etna basalt using 3D acoustic-emission location and X-ray computed tomography. Geophysical Research

385   Letters, 34(3), 2007.

Brace, W. F., and Bombolakis, E. G.: A note on brittle crack growth in compression. Journal of Geophysical Research, 68(12), 3709–3713. doi:10.1029/JZ068i012p03709, 1963.

Brantut, N.: Dilatancy-induced fluid pressure drop during dynamic rupture: Direct experimental evidence and consequences for earthquake dynamics. Earth and Planetary Science Letters, 538, 116179, 2020.

390   Chinnery, M. A., and Petrak, J. A.: The dislocation fault model with a variable discontinuity, Tectonophysics, 5(6), 513–529, doi:10.1016/0040-1951(68)90008-5, 1968.

Cooke, M. L., and Underwood, C. A.: Fracture termination and step-over at bedding interfaces due to frictional slip and interface opening. Journal of Structural Geology, 23(2-3), 223-238, 2001.

Crider, J. G., and Peacock, D. C.: Initiation of brittle faults in the upper crust: a review of field observations. Journal of

395   Structural Geology, 26(4), 691-707, 2004.

Davy, P., Goc, R., Darcel, C., Bour, O., Dreuzy, J., and Munier, R.: A likely universal model of fracture scaling and its consequence for crustal hydromechanics, Journal of Geophysical Research: Solid Earth, 115(B10), 1–13, doi:10.1029/2009jb007043, 2010.

Davy, P., Le Goc, R., and Darcel, C.: A model of fracture nucleation, growth and arrest, and consequences for fracture density

400   and scaling, Journal of Geophysical Research: Solid Earth, 118, 1393–1407, doi:10.1002/jgrb.50120, 2013.

Del Castello, M., and Cooke, M. L.: Underthrusting-accretion cycle: Work budget as revealed by the boundary element method, Journal of Geophysical Research: Solid Earth, 112, B12404, doi:10.1029/2007JB004997, 2007.

Du, Y., and Aydin, A.: The maximum distortional strain energy density criterion for shear fracture propagation with applications to the growth paths of enechelon faults. Geophysical Research Letters, 20(11), 1091-1094, 1993.

405   Fattaruso, L. A., Cooke, M. L., Dorsey, R. J., and Housen, B. A.: Response of deformation patterns to reorganization of the southern San Andreas fault system since ca. 1.5 Ma. Tectonophysics, 693, 474-488, 2016.

French, M. E., and Zhu, W.: Slow fault propagation in serpentinite under conditions of high pore fluid pressure. Earth and Planetary Science Letters, 473, 131-140, 2017.

Griffith, A. A.: VI. The phenomena of rupture and flow in solids. Philosophical Transactions of the Royal Society of London.

410   Series A, containing papers of a mathematical or physical character, 221(582-593), 163-198, 1921.

Harding, T. P.: Seismic characteristics and identification of negative flower structures, positive flower structures, and positive structural inversion. AAPG Bulletin, 69(4), 582-600, 1985.

Herbert, J. W., Cooke, M. L., Souloumiac, P., Madden, E. H., Mary, B. C., and Maillot, B.: The work of fault growth in laboratory sandbox experiments. Earth and Planetary Science Letters, 432, 95-102, 2015.

415 Ikari, M. J., Saffer, D. M., and Marone, C.: Frictional and hydrologic properties of clay-rich fault gouge. Journal of Geophysical Research-Solid Earth, 114, B05409, doi:10.1029/2008JB006089, 2009.

Irwin, G.: Analysis of stresses and strains near the end of a crack traversing a plate. Journal of Applied Mechanics 24, 361–364, 1957.

Isida, M.: Effect of width and length on stress intensity factors of internally cracked plates under various boundary
420 conditions. International Journal of Fracture Mechanics, 7(3), 301-316, 1971.

Jackson, C. A. L., and Rotevatn, A.: 3D seismic analysis of the structure and evolution of a salt-influenced normal fault zone: a test of competing fault growth models. Journal of Structural Geology, 54, 215-234, 2013.

Jaeger, J. C., Cook, N. G. W., and Zimmerman, R.: Rock mechanics. Fundamentals of Rock Mechanics. Chapman and Hall, London, 1979.

425 Kandula, N., Cordonnier, B., Boller, E., Weiss, J., Dysthe, D. K., and Renard, F.: Dynamics of microscale precursors establish brittle-compressive failure as a critical phenomenon in Carrara marble. Journal of Geophysical Research, 124, 6121-6139, doi:10.1029/2019JB017381, 2019.

Kawakata, H., Cho, A., Yanagidani, T., and Shimada, M.: The observations of faulting in Westerly granite under triaxial compression by X-ray CT scan. International Journal of Rock Mechanics and Mining Sciences, 34(3-4), 151-e1, 1997.

430 Lin, P., Wong, R. H., and Tang, C. A.: Experimental study of coalescence mechanisms and failure under uniaxial compression of granite containing multiple holes. International Journal of Rock Mechanics and Mining Sciences, 77, 313-327, 2015.

Lisabeth, H. and Zhu, W.: Effect of temperature and pore fluid on the strength of porous limestone. Journal of Geophysical Research, 120, 6191–6208, doi:10.1002/2015JB012152, 2015.

Lockner, D., Byerlee, J. D., Kuksenko, V., Ponomarev, A., and Sidorin, A.: Quasi-static fault growth and shear fracture energy
435 in granite. Nature, 350(6313), 39-42, 1991.

Madden, E. H., Cooke, M. L., and McBeck, J.: Energy budget and propagation of faults via shearing and opening using work optimization. Journal of Geophysical Research: Solid Earth, 122(8), 6757-6772, 2017.

Mair, K., Elphick, S., and Main, I.: Influence of confining pressure on the mechanical and structural evolution of laboratory deformation bands. Geophysical Research Letters, 29(10), 49-1, 2002.

440   Mansfield, C., and Cartwright, J.: Fault growth by linkage: observations and implications from analogue models. Journal of Structural Geology, 23(5), 745-763, 2001.

Mary, B. C. L., Maillot, B., and Leroy, Y. M.: Deterministic chaos in frictional wedges revealed by convergence analysis. International Journal for Numerical and Analytical Methods in Geomechanics, 37(17), 3036-3051, 2013.

McBeck, J., Cooke, M., and Fattaruso, L.: Predicting the propagation and interaction of frontal accretionary thrust faults with
445   work optimization. Tectonophysics, 228461, 2020.

McBeck, J., Cooke, M., and Madden, E.: Work optimization predicts the evolution of extensional step overs within anisotropic host rock: Implications for the San Pablo Bay, CA. Tectonics, 36(11), 2630-2646, 2017.

McBeck, J., Kandula, N., Aiken, J. M., Cordonnier, B., and Renard, F.: Isolating the Factors That Govern Fracture Development in Rocks Throughout Dynamic In Situ X-Ray Tomography Experiments. Geophysical Research Letters, 46(20),
450   11127-11135, 2019a.

McBeck, J., Mair, K., and Renard, F.: How porosity controls macroscopic failure via propagating fractures and percolating force chains in porous granular rocks. Journal of Geophysical Research: Solid Earth, 124(9), 9920-9939, 2019b.

Menéndez, B., Zhu, W., and Wong, T. F.: Micromechanics of brittle faulting and cataclastic flow in Berea sandstone. Journal of Structural Geology, 18(1), 1-16, 1996.

455   Müller, G.: Starch columns: Analog model for basalt columns. Journal of Geophysical Research: Solid Earth, 103(B7), 15239-15253, 1998.

Narr, W., and Suppe, J.: Joint spacing in sedimentary rocks. Journal of Structural Geology, 13(9), 1037-1048, 1991.

Okubo, C. H., and Schultz, R. A.: Evolution of damage zone geometry and intensity in porous sandstone: insight gained from strain energy density. Journal of the Geological Society, 162(6), 939-949, 2005.

460   Olson, J. E.: Joint pattern development: Effects of subcritical crack growth and mechanical crack interaction. Journal of Geophysical Research: Solid Earth, 98(B7), 12251-12265, 1993.

Olson, E. L., and Cooke, M. L.: Application of three fault growth criteria to the Puente Hills thrust system, Los Angeles, California, USA. Journal of Structural Geology, 27(10), 1765-1777, 2005.

Ougier-Simonin, A. and Zhu, W.: Effect of pore pressure build-up on slowness of rupture propagation. Journal of Geophysical
465   Research, 120, 7966–7985, 10.1002/2015JB012047, 2015.

Ougier-Simonin, A. and Zhu, W.: Effects of pore fluid pressure on slip behaviors: an experimental study. Geophysical Research Letters, 40, 2619-2624, 10.1002/grl.50543, 2013.

Paterson, M. S., and Wong, T. F.: Experimental rock deformation-the brittle field. Springer Science and Business Media, 2005.

Peng, S., and Johnson, A. M.: Crack growth and faulting in cylindrical specimens of Chelmsford granite. In International
470   Journal of Rock Mechanics and Mining Sciences and Geomechanics Abstracts (Vol. 9, No. 1, pp. 37-86). Pergamon, 1972.

Pollard, D. D., and Aydin, A.: Progress in understanding jointing over the past century. Geological Society of America
Bulletin, 100(8), 1181-1204, 1988.

Reches, Z. E., and Lockner, D. A.: Nucleation and growth of faults in brittle rocks. Journal of Geophysical Research: Solid
Earth, 99(B9), 18159-18173, 1994.

475   Renard, F.: Critical evolution of damage towards system size failure in a crystalline rock [Data set]. Norstore.
doi:10.11582/2017.00025, 2017.

Renard, F.: Volumetric and shear processes in crystalline rock during the approach to faulting [Data set]. Norstore.
doi:10.11582/2018.00023, 2018.

Renard, F., Cordonnier, B., Dysthe, D. K., Boller, E., Tafforeau, P., and Rack, A.: A deformation rig for synchrotron
480   microtomography studies of geomaterials under conditions down to 10 km depth in the Earth. Journal of Synchrotron
Radiation, 23(4), 1030-1034, 2016.

Renard, F., McBeck, J., Cordonnier, B., Zheng, X., Kandula, N., Sanchez, J. R., Kobchenko, M., Noiriel, C., Zhu, W., Meaken,
P., and Fusseis, F.: Dynamic in situ three-dimensional imaging and digital volume correlation analysis to quantify strain
localization and fracture coalescence in sandstone. Pure and Applied Geophysics, 176(3), 1083-1115, 2019a.

485   Renard, F., McBeck, J., Kandula, N., Cordonnier, B., Meakin, P., Ben-Zion, Y.: Volumetric and shear processes in crystalline
rock approaching faulting. Proceedings of the National Academy of Sciences, 116, 16234-16239, doi:
10.1073/pnas.1902994116, 2019b.

Renard, F., Weiss, J., Mathiesen, J., Ben-Zion, Y., Kandula, N., and Cordonnier, B.: Critical evolution of damage toward
system-size failure in crystalline rock. Journal of Geophysical Research: Solid Earth, 123(2), 1969-1986, 2018.

490   Rice, J. R.: On the stability of dilatant hardening for saturated rock masses. Journal of Geophysical Research, 80(11), 1531–
1536. doi:10.1029/JB080i011p01531, 1975.

Rudnicki, J. W., and Chen, C. H.: Stabilization of rapid frictional slip on a weakening fault by dilatant hardening. Journal of
Geophysical Research, 93(B5), 4745–4757. doi:10.1029/JB093iB05p04745, 1988.

Segall, P., and Pollard, D. D.: Mechanics of discontinuous faults. Journal of Geophysical Research, 85, 4337–4350,
495   doi:10.1029/JB085iB08p04337, 1980.

Stanchits, S., Vinciguerra, S., and Dresen, G.: Ultrasonic velocities, acoustic emission characteristics and crack damage of
basalt and granite. Pure and Applied Geophysics, 163(5-6), 975-994, 2006.

Underwood, C. A., Cooke, M. L., Simo, J. A., and Muldoon, M. A.: Stratigraphic controls on vertical fracture patterns in Silurian dolomite, northeastern Wisconsin. AAPG Bulletin, 87(1), 121-142, 2003.

500   Wesnousky, S. G.: Predicting the endpoints of earthquake ruptures. Nature, 444(7117), 358-360, 2006.

Wong, T. F., David, C., and Zhu, W.: The transition from brittle faulting to cataclastic flow in porous sandstones: Mechanical deformation. Journal of Geophysical Research: Solid Earth, *102*(B2), 3009-3025, 1997.

Wu, H., and Pollard, D.D.: An experimental study of the relationship between joint spacing and layer thickness. Journal of Structural Geology, 17(6), 887-905, 1995.

505   Xing, T., Zhu, W., French, M., and Belzer, B.: Stabilizing Effect of High Pore Fluid Pressure on Slip Behaviors of Gouge-bearing Faults. Journal of Geophysical Research: Solid Earth, 124(9), 9526-9545, 2019.

Xing, T., Zhu, W., Fusseis, F., and Lisabeth, H.: Generating porosity during olivine carbonation via dissolution channels and expansion cracks, Solid Earth, doi:10.5194/se-9-879-2018, 2018.

Zhu, W., Baud, P. and Wong, T.F.: Micromechanics of cataclastic pore collapse in limestone. Journal of Geophysical Research:
510   Solid Earth, 115(B4), doi:10.1029/2009JB006610, 2010.
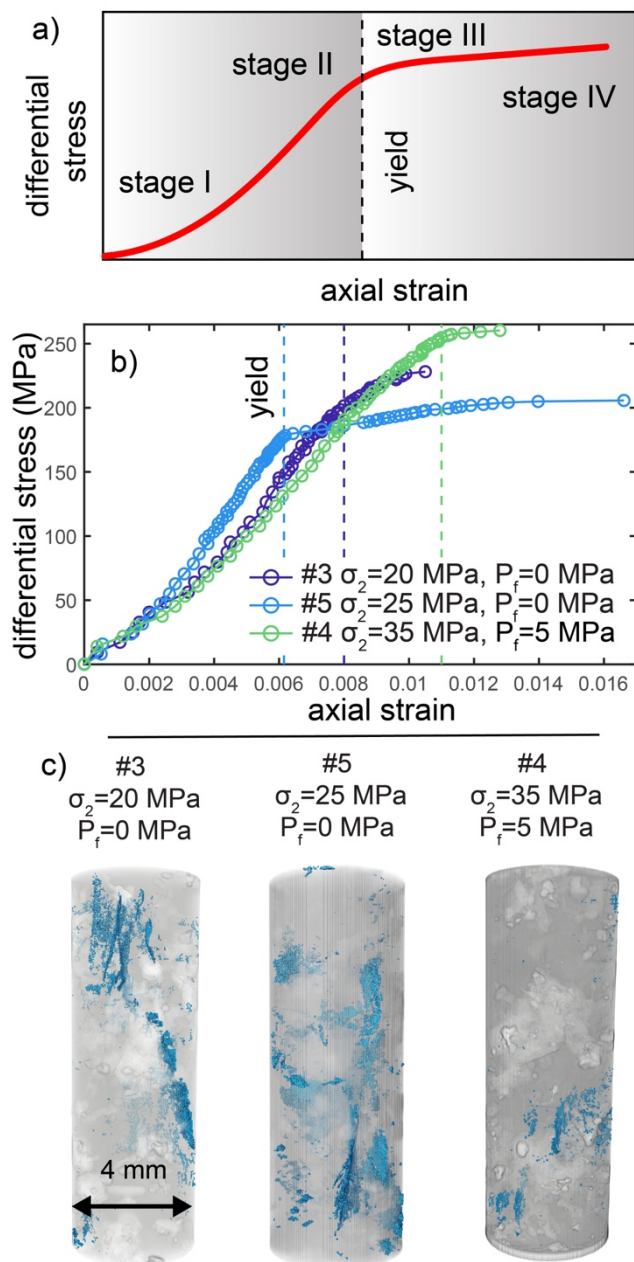
Figure 1: Macroscopic behavior of each experiment produced by fracture network development. a) Macroscopic stages of deformation. Stage I is the initial non-linear stage corresponding to the closure of pre-existing defects. Stage II includes the quasi-linear relationship between stress and strain, when the deformation can be approximated as elastic. Stage III occurs when deformation behavior deviates significantly from linear elasticity. The yield point marks the boundary between stages II and III. Stage IV occurs close to macroscopic failure, when the effective elastic modulus is near zero. The timing of the transition between stages I and II, and stages III and IV will remain qualitative in this analysis. b) Differential stress and axial strain relationships of each experiment. Circles show the conditions when a tomogram was acquired. The applied confining stress and pore fluid pressure increase from monzonite #3 ($\sigma_2 = 20\ MPa, P_f = 0$), #5 ($\sigma_2 = 25\ MPa, P_f = 0$) and #4 ($\sigma_2 = 35\ MPa, P_f = 5\ MPa$). c) Fracture geometry at final scan. Fractures shown in blue, minerals shown with transparent grey and white. The fracture network geometry in the last scan acquired before macroscopic failure includes longer and more volumetric fractures in the experiments with $\sigma_2 = 20 - 25\ MPa$ and $P_f = 0$ (#3, #5) than in the experiment with $\sigma_2 = 35\ MPa, P_f = 5\ MPa$ (#4).
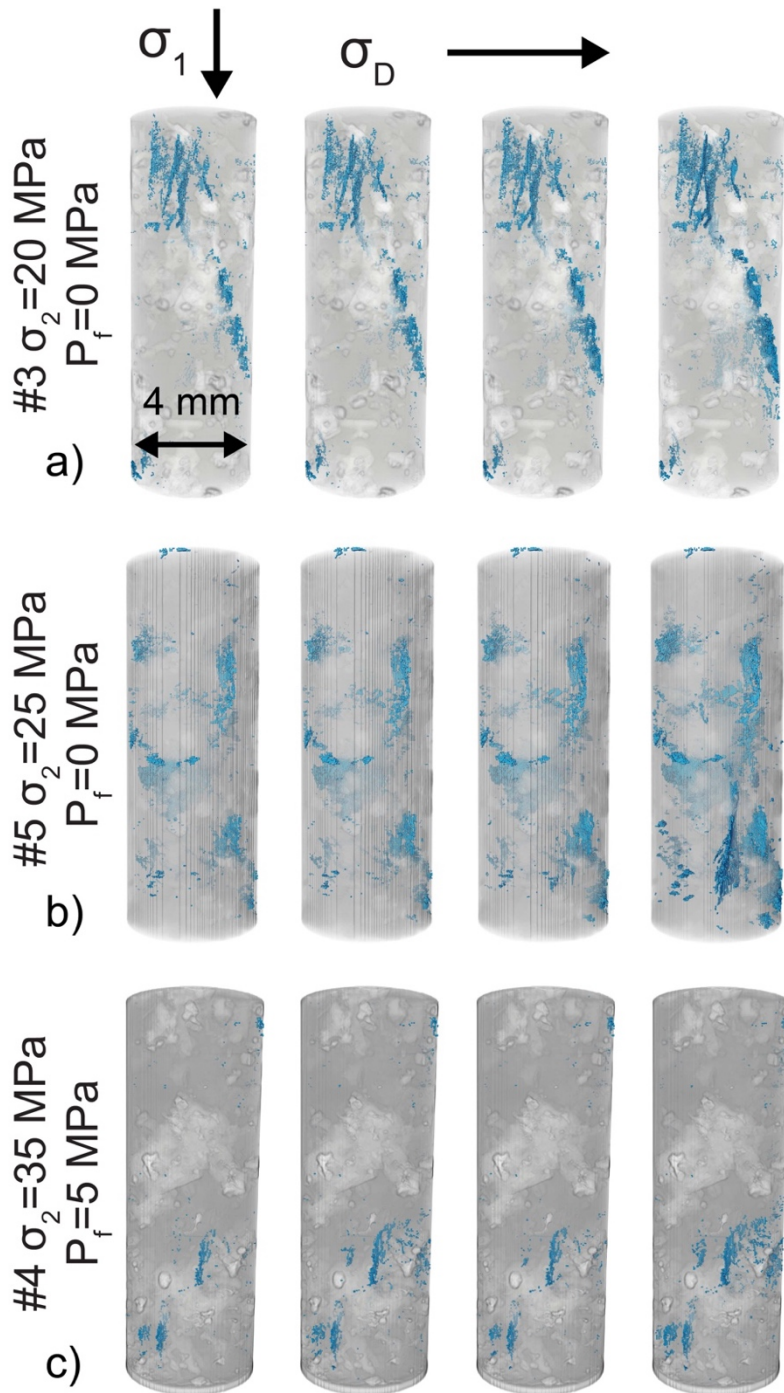
Figure 2: Evolving fracture networks in the final four loading steps of each experiment before system-size failure.

540
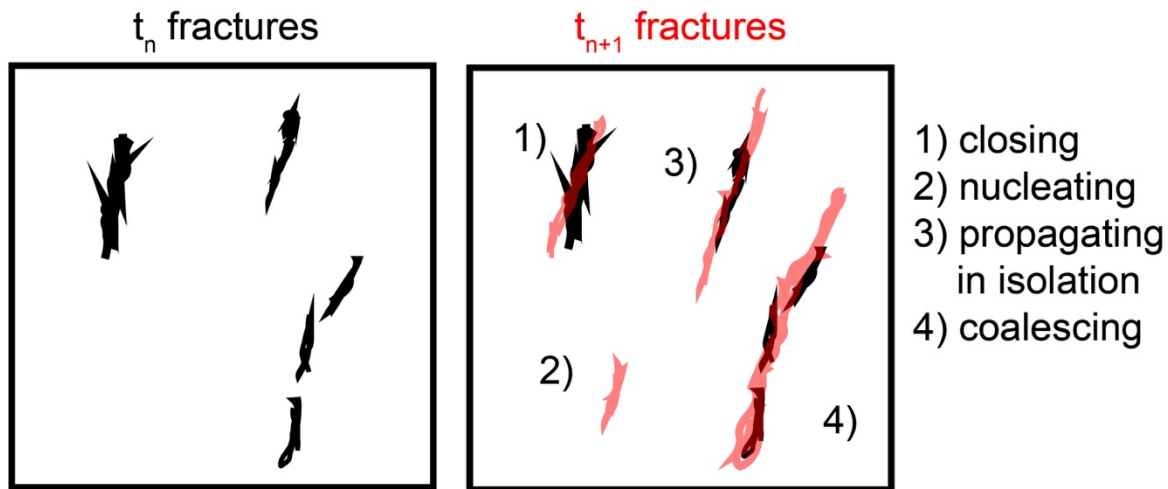
Figure 3: Modes of fracture network development captured by algorithm. By tracking individual fractures in sequential scans, we can identify fractures that 1) close, 2) nucleate, 3) propagate in isolation and 4) coalesce from one time to the next, t_n to t_{n+1}.

545
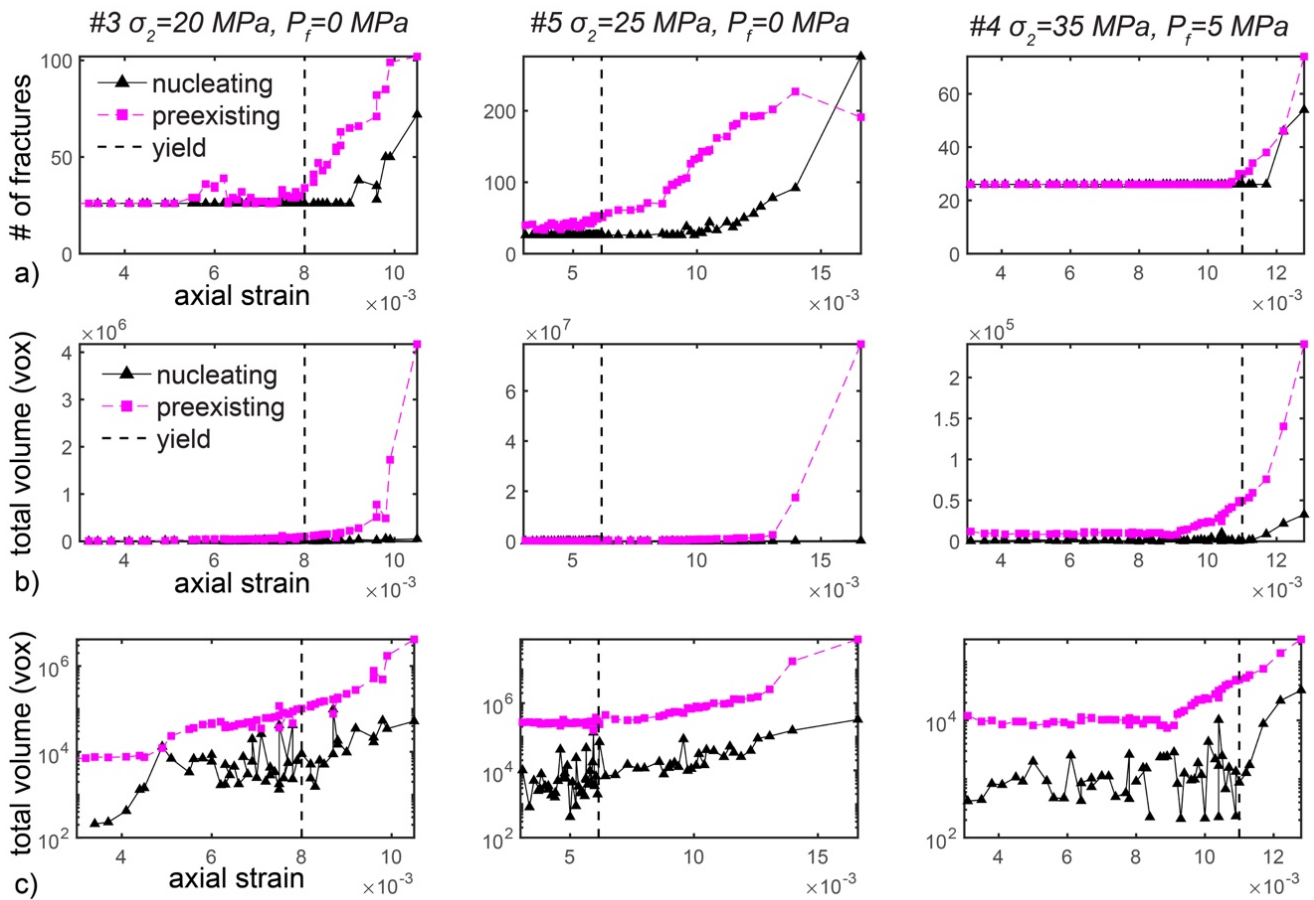
Figure 4: The competing influence of fracture nucleation and preexisting growth in each experiment. The applied effective pressure (confining pressure minus pore fluid pressure) increases from left to right. a) The number of fractures identified as nucleating or preexisting in each loading step. The total volume of the nucleating and preexisting fractures in linear b) and log-linear c) space. Dashed vertical lines show the axial strain at the macroscopic yielding point identified from the shallowing of the stress-strain curves
550 **(Figure 1), separating stages I-II and III-IV. The total volume of preexisting fractures exceeds the volume of newly nucleating fractures in the final loading steps preceding macroscopic failure, indicating the dominance of preexisting development rather than nucleation. The uptick of nucleating fractures after yield is more significant in the water-saturated sample compared to the nominally dry samples.**

555
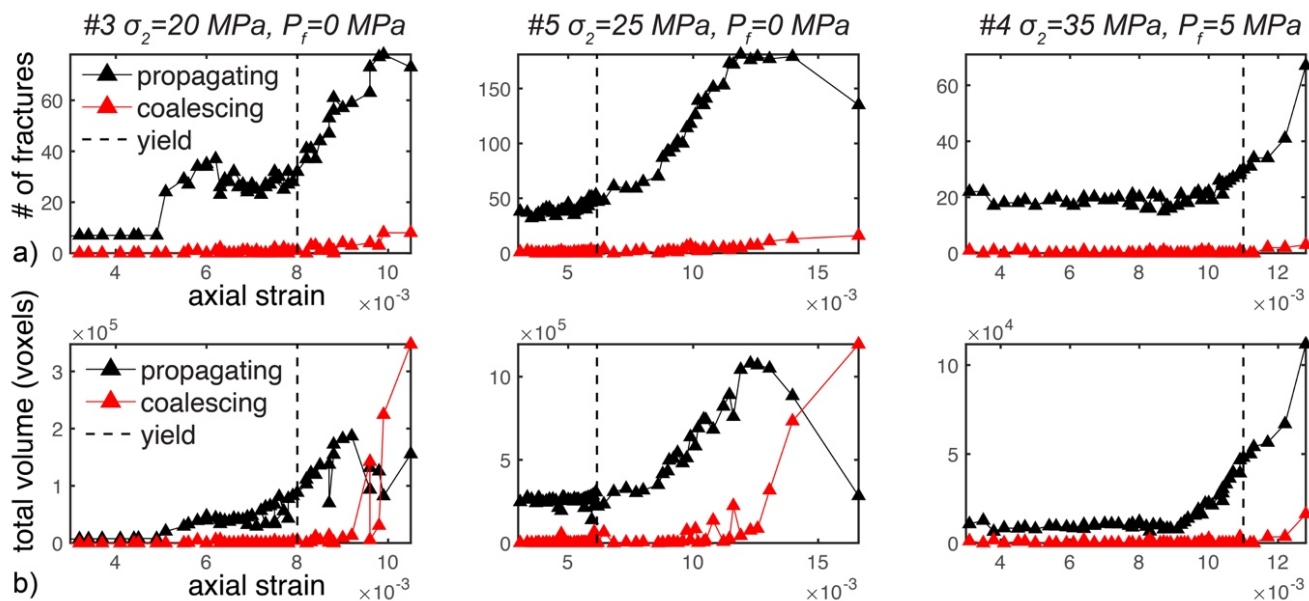
Figure 5: The varying influence of preexisting fracture coalescence and propagation. a) The number of fractures propagating in isolation (black) and coalescing (red). b) The total volume of fractures propagating in isolation or coalescing. Prior to macroscopic failure, the total volume of propagating fractures decreases and the total volume of coalescing fractures increases in the nominally dry experiments (#3 and #5), indicating the dominance of coalescence rather than isolated propagation. In comparison, in the water-saturated experiments, the propagating fractures dominate throughout loading.

560
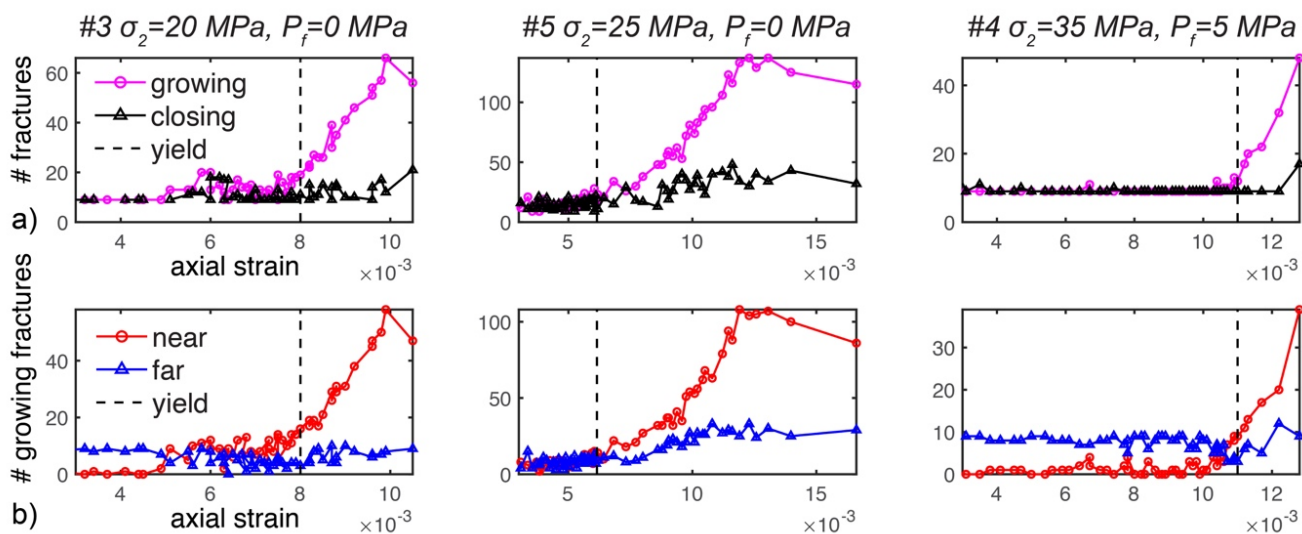
Figure 6: The influence of stress perturbations and localization on fracture growth. a) The number of growing (magenta, circles) and closing (black, triangles) fractures. b) The number of growing fractures that do (near, red circles) and do not (far, blue triangles) have other fractures within one fracture length of them throughout loading. For example, if one fracture (fracture #1) is located within *y* distance of another fracture (#2) with length *y*, then fracture #1 is counted in the near category. LEFM predicts that fractures that are located within a length of another fracture should be more likely to grow than fracture located further away. Our observations match this expectation following the macroscopic yield point, when the number of growing fractures located near to other fractures exceeds the number located far from others.

565
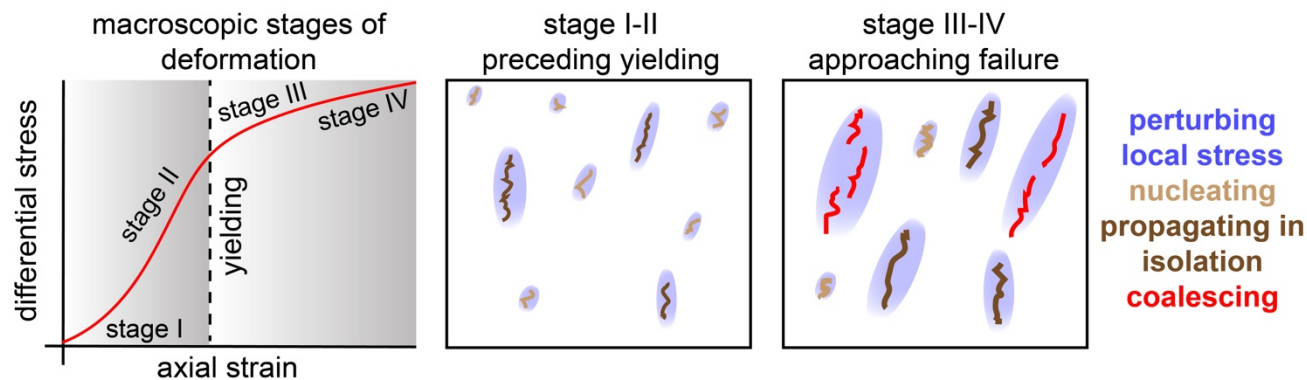
Figure 7: Schematic of varying modes of fracture development observed preceding yielding and approaching macroscopic failure. When the rock experiences lower differential stress and the fracture network is more distributed, 1) similar numbers of new fractures nucleate and preexisting fractures grow, 2) isolated propagation dominates coalescence, and 3) local stress perturbations do not appear to promote fracture growth. When the approaches macroscopic failure, 1) preexisting fracture propagation dominates new fracture nucleation, 2) coalescence dominates isolated propagation shortly before macroscopic failure in the experiments with the lowest confining stress, and 3) local stress perturbations promote fracture growth.